OPEN ACCESS

University of BRISTOL

Jeffrey, M. R., & Avrutin, V. (2022). Periods 1+2 implies chaos in steep or nonsmooth maps. *Nonlinearity*, *35*(12). https://doi.org/10.1088/1361-6544/ac9506

Publisher's PDF, also known as Version of record

License (if available):
CC BY

Link to published version (if available):
10.1088/1361-6544/ac9506

Link to publication record in Explore Bristol Research
PDF-document

This is the final published version of the article (version of record). It first appeared online via IOP Publishing at https://doi.org/10.1088/1361-6544/ac9506 . Please refer to any applicable terms of use of the publisher.

University of Bristol - Explore Bristol Research
General rights

This document is made available in accordance with publisher policies. Please cite only the published version using the reference above. Full terms of use are available:
http://www.bristol.ac.uk/red/research-policy/pure/user-guides/ebr-terms/

OPEN ACCESS
IOP Publishing | London Mathematical Society Nonlinearity
Nonlinearity **35** (2022) 6014–6041 https://doi.org/10.1088/1361-6544/ac9506

Periods 1 + 2 imply chaos in steep or nonsmooth maps

Mike R Jeffrey[1,*] **and Viktor Avrutin**[2]

[1] Department of Engineering Mathematics, University of Bristol, Ada Lovelace Building, Bristol BS8 1TW, United Kingdom
[2] Institute for Systems Theory and Automatic Control, University of Stuttgart, Pfaffenwaldring 9, 70550 Stuttgart, Germany

E-mail: mike.jeffrey@bristol.ac.uk

Received 22 September 2021, revised 22 July 2022
Accepted for publication 26 September 2022
Published 17 October 2022

Abstract

Maps with discontinuities can be shown to have many of the same properties of continuous maps if we include *hidden orbits*—solutions that include points lying on a discontinuity. We show here how the well known property that 'period 3 implies chaos' also applies to maps with discontinuities, but with a twist, namely that if a map has a hidden fixed point and a hidden period 2 orbit, then it has hidden orbits of all periods, or concisely 'period 1 + 2 implies chaos'. More precisely we show that for a one-dimensional map defined on an interval, if there exist hidden orbits of periods p and q, then there exist hidden orbits of all periods $ap + bq$, for any $a, b \in \mathbb{N}$. To better understand this result we show that, by smoothing or 'regularising' across the discontinuity, these hidden orbits become regular unstable orbits, and the familiar results for continuous maps (like 'period 3 implies chaos') are restored. We also show examples of hidden orbits in some applications of oscillators, and consider how these results can be used to approximate the behaviour of continuous maps with steep segments.

Keywords: nonsmooth map, steep map, discontinuous, Sharkovskii, hidden, periodic orbits

Mathematics Subject Classification numbers: 37E05, 39A28, 26E25, 49J52.

(Some figures may appear in colour only in the online journal)

*Author to whom any correspondence should be addressed.
Recommended by Dr Lorenzo J Diaz.

Original content from this work may be used under the terms of the Creative Commons Attribution 3.0 licence. Any further distribution of this work must maintain attribution to the author(s) and the title of the work, journal citation and DOI.

1. Introduction

Continuous and discontinuous maps are subject to seemingly very different laws governing their dynamics, particularly the periodicities and the bifurcations they exhibit. Yet in [18] it was suggested that these differences are largely removed by considering the *hidden dynamics* associated with discontinuities. If, for instance, a discontinuity in a one-dimensional map $x_{n+1} = f(x_n)$ is replaced with a vertical branch, so that the graph of f is connected but set-valued, then the two maps are topologically semi-conjugate, see e.g. figure 1(i). The dynamics of the *connected* map preserves all of the dynamics of the discontinuous map, but in addition the connected map involves *hidden orbits* that have iterates on the vertical branch at the discontinuity.

In [15, 18] it was shown that these hidden orbits provide unstable branches that literally 'fill the gaps' left by discontinuities in bifurcation diagrams. In the present paper we investigate the role that hidden dynamics plays in determining the periods of orbits that exist in a map.

Maps with discontinuities arise from several sources in dynamical systems. They appear in return maps when a Poincaré section is tangent to the flow [20], or straddles a separatrix such as the stable manifold to a saddle in the Cherry flow or Lorenz semi-flow [12, 18, 23, 30, 31]. They can also occur simply because a discrete time model switches from one continuous mode of behaviour to another as in [29], and can be considered as approximating smooth maps with steep change, see e.g. [24]. A common source of maps with discontinuities this century has been between parts of a flow that hit or miss a threshold where the system behaviour changes, as happens in mechanical impact or friction oscillators [6, 13, 19], in electronic controllers [8, 26], or in physiological applications like sleep-wake regulation, heart arrhythmia, or mitosis, see e.g. [5, 7, 9]. We will look more closely at some examples in section 4.

With such varied applications as these, the choice of how to define a map and its orbits at a discontinuity are a modelling problem as well as a theoretical curiosity. One extreme is to say that orbits are ill-defined at a discontinuity. Another extreme is to define orbits as being set-valued, as may be natural in interval-arithmetic or fuzzy-logic. But it is often desirable to take an intermediate approach, and retain the notion of an orbit being a sequence of distinct points even when it encounters a discontinuity.

A hidden orbit is simply a solution of a map that has one or more iterates at a discontinuity, defined by allowing the map to take any one of a set of values, with those values taken from a vertical branch in its graph (e.g. the orbit with period 2 shown in figure 1(ii)). They offer a relatively simple analytic tool, not only for adding to our knowledge of discontinuous maps, but also, as we will discuss later in this paper, for approximating continuous maps with steep segments.

One particular result for one dimensional maps that appears to require continuity is Sharkovskii's theorem [25]. This says that if a continuous one-dimensional map $f : U \to U$, where $U \subset \mathbb{R}$, has a cycle of period p, then it also has a cycle of every period k left of p (written $k \prec p$) in Sharkovkii's ordering

$$1 \prec 2 \prec 2^2 \prec 2^3 \prec \ldots \prec 2^n \prec \ldots \quad \ldots \prec 7\cdot 2^n \prec 5\cdot 2^n \prec 3\cdot 2^n \prec \ldots$$
$$\ldots \prec 7\cdot 2 \prec 5\cdot 2 \prec 3\cdot 2 \prec \ldots \prec 9 \prec 7 \prec 5 \prec 3.$$

The more quotable corollary of this is that 'period 3 implies chaos' in a continuous map on an interval [21]. If f has a discontinuity then we cannot apply Sharkovskii's theorem in its original form, and there are obvious counterexamples showing that the ordering does not apply. The

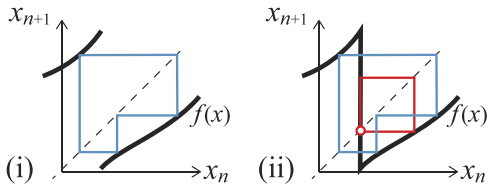

Figure 1. The discontinuous map shown in (i) has a stable cycle of period 3 (blue). By including the vertical branch at the discontinuity we obtain the connected map (ii), which in addition has a hidden cycle of period 2 (red) and a hidden fixed point (red circle).

discontinuous map in figure 1(i), for example, has a stable cycle of period 3, but has no other regular cycles, so it does not appear to fulfil the Sharkovskii ordering.

We shall show that Sharkovskii's ordering is restored if we include hidden orbits, but with an added twist. We show that if a map has a hidden fixed point and a hidden cycle of period 2, then it has orbits of all periods, or simply '*periods* $1+2$ *imply chaos*'.

In the example of figure 1(i), hidden orbits can be introduced by including the vertical branch across the discontinuity to obtain the connected map in figure 1(ii). This has a hidden cycle of period 2 and a hidden fixed point.

The curiosity that concerns us here is that when a pair of hidden cycles exist, like the cycles of period 2 and 1 in figure 1(ii), they generate a countable infinity of distinct cycles that are formed by 'hopping' between the pair at the discontinuity. We define this 'hopping' as just the concatenation of cycles in section 2. Whenever a hidden cycle passes through a discontinuity, it may continue around the same cycle, or 'hop' to a new one. At first this may seem to make the existence of hidden cycles of higher periods arbitrary, but we shall see that it occurs in precisely the manner necessarily to fulfil results like Sharkovskii's ordering. More precisely, the existence of hidden orbits of periods p and q, that pass through the same discontinuity, generates cycles of all periods $ap+bq$ for any $a, b \in \mathbb{N}$.

We set out basic definitions for hidden cycles and their concatenations, in section 2. As a direct consequence we show that a hidden cycle of period 2 accompanied by a hidden fixed point implies cycles of all periods. While this may appear somewhat arbitrary, in section 3 we will show how it creates a correspondence to the cycles of continuous maps.

In particular we show precisely how the rule above, that '*periods* $1+2$ *imply chaos*' for a connected map, is consistent with the classic result that '*period 3 implies chaos*' for a continuous map. Taking a continuous piecewise-monotonic map with a steep segment, we show that existence of a hidden period 2 orbit and hidden fixed point, at a vertical branch, imply the existence of a nearby cycle of period 3 in a continuous map with a steep segment. We also show the converse, that cycles with odd or even periods, with iterates on the steep segment of a continuous map, collapse onto a hidden cycle of period 2 as the steep segment is made vertical.

In section 4 we illustrate hidden orbits in some basic oscillators from applications to mechanical and living systems. In section 5 we discuss the interpretation of hidden orbits in physical applications, and discuss their use to approximate the dynamics of continuous maps with steep segments, before some concluding remarks in section 6.

In illustrations we shall occasionally make use of the Heaviside step function $\Theta(x)$ in the form

$$\Theta(x) = \left\{ \begin{array}{ll} 1 & \text{for } x > 0 \\ 0 & \text{for } x < 0 \end{array} \right\}, \qquad \Theta(0) \in [0,1], \tag{1}$$

that is, at $x = 0$ the function Θ can take any value on the interval $[0, 1]$.

2. Hidden orbits and concatenations

We begin by setting out a few definitions concerning hidden orbits, the way they form cycles, and the way these can be concatenated to form new cycles. It will follow directly from these definitions that maps with hidden cycles obey Sharkovskii's ordering and that, if a hidden fixed point is present to provide arbitrary concatenations, then periods $1+2$ imply chaos.

Consider a map

$$x_{n+1} = f(x_n) \tag{2a}$$

where f is continuous except at a countable number of points $x = X_1, X_2, \ldots$. At each point X_i let the value of f satisfy

$$f(X_i) \in F_i \quad \text{such that } F_i^{\pm} := \lim_{\varepsilon \to 0} f(X_i \pm \varepsilon) \in F_i, \tag{2b}$$

where F_i is a connected set, and the limits $F_i^{\pm}$ exist by the continuity of f. We refer to F_i as the *vertical branch* of f at X_i. The simplest choice of vertical branch is the interval $F_i = \left[F_i^-, F_i^+\right]$, but we will show later that other choices are sometimes required. We refer to f as a *connected* map (distinguishing it from a *discontinuous map* where F_i is not a connected set and need not be defined at all).

Our main concern here will be maps for which $F_i^- \neq F_i^+$. For example, a map with $f(x) = 2\Theta(x) - 1 - x$ on $|x| < 1$ has a step at $X_1 = 0$, where $F_i^{\pm} = \pm 1$ and $F_1 = [-1, +1]$. The results we derive can also be applied if $F_i^+ = F_i^-$ but the map is not uniquely defined at X_i. The second iterate $f^2(x)$ of this same example has such a point at $X_1 = 0$, as it is the identity $f^2(x) = x$ for all $x \neq X_1$, but lies on a set $f^2(X_1) \in [-1, +1]$ at X_1. Other examples can be found in the context of multi-valued maps, see e.g. [2, 3].

The vertical branches F_i at the points X_i are responsible for generating hidden orbits.

Definition 2.1. A **hidden orbit** of a map $x_{n+1} = f(x_n)$ is an iterate sequence $\{x_1, x_2, \ldots\}$ with at least one point $x_n = X_i$ at which f has a vertical branch F_i, such that $x_{n+1} \in F_i$, for some $n, i \in \mathbb{N}$.

From any point $x_n = X_i$ that lies at a discontinuity, the next point can take one of infinitely many different values $x_{n+1} \in F_i$, generating an uncountable number of forward orbits. It may occur that one or more of these orbits returns to the same discontinuity, $x_{n+p} = X_i$ for some $p > 0$, which *may* form a period p orbit, or simply a *p-cycle*.

Definition 2.2. A **hidden *p*-cycle** of a map $x_{n+1} = f(x_n)$ is a hidden orbit such that $x_{n+p} = x_p$ for any $n \in \mathbb{N}$.

A *1-cycle* will usually be called a *fixed point*. For example, figure 1 shows a regular three-cycle, a hidden two-cycle, and a hidden fixed point. Note, however, that just because an orbit with $x_n = X_i$ returns to $x_{n+p} = X_i$ for some $p > 0$, does not necessarily mean this orbit *is* a p-cycle. The next point $x_{n+p+1} \in F_i$ again generates uncountably many onward trajectories, only one of which will be the p-cycle, among countably many other cycles and uncountably many other non-periodic orbits.

For example consider the map $x_{n+1} = x_n + 5 - 7\Theta(x_n)$. The point $x_n = 0$ maps to $x_{n+1} \in [-2, +5]$, and as such this point $x_n = 0$ occurs as an iterate in uncountably many distinct orbits. Among these are three different hidden cycles $\{0\}$, $\{0, 2\}$, and $\{0, 4, 2\}$. Note that although these cycles have a common point at $x = 0$, they are distinct trajectories of the map because their sequences are different, namely with periods 1, 2, and 3, respectively.

Similarly to regular cycles, the following notion is useful.

Definition 2.3. A hidden p-cycle is **irreducible** if its iterate sequence $\{x_1, \ldots, x_p\}$ does not consist of r repetitions of a periodic sequence of shorter length $m = p/r$ for $m, p, r \in \mathbb{N}$, $r > 1$.

All of the cycles shown in figure 1 are obviously irreducible.

Hidden cycles may be irreducible and yet visit the same discontinuity multiple times, so a further notion is useful.

Definition 2.4. A **primary *p*-cycle** of a map $x_{n+1} = f(x_n)$ is an iterate sequence $\{x_1, x_2, \ldots, x_p\}$ in which each point $x_n = X_i$ occurs at most once, that is $x_n = X_i$ implies $x_m \neq X_i$ for all $m \neq n$, $m, n \in \mathbb{N}$.

A hidden orbit that is primary can only visit a given discontinuity once, hence it cannot be split into two or more identical subsequences, hence a primary orbit is irreducible.

Unlike continuous maps, it is possible for orbits of (2) to be distinct, and yet share a common iterate on a point of discontinuity X_i. Any sequence that is a solution of (2) ending at X_i, can be concatenated with any sequence that is a solution of (2) starting with some $x \in F_i$, to form uncountably many solution sequences of (2), i.e. hidden orbits. We are most interested in how this applies to cycles.

Definition 2.5. If two hidden cycles of a map have sequences

$$\{X_i, x_2, x_3, \ldots, x_p\} \quad \text{and} \quad \{X_i, y_2, y_3, \ldots, y_q\}$$

for some $p, q \in \mathbb{N}$ and $x_2 \neq y_2$, $x_2, y_2 \in F_i$, then their **concatenation** is a hidden $(p+q)$-cycle, defined as the sequence

$$\{X_i, x_2, x_3, \ldots, x_p, X_i, y_2, y_3, \ldots, y_q\}.$$

The fact that the resulting sequence forms a cycle follows from the same property that allows concatenation, namely that since both of the original orbits are cycles, both x_p and y_q map to X_i. (Note that, as we remarked after definition 2.2, there also exist uncountably many other non-periodic orbits in which these sequences appear, but these are not our interest here.)

The concatenation of non-identical irreducible orbits need not itself be irreducible. For example consider concatenating a two-cycle $\{X_i, x_2\}$ with a six-cycle $\{X_i, x_3, X_i, x_2, X_i, x_3\}$, where $x_2 \neq x_3$, to form the sequence

$$\{X_i, x_3, X_i, x_2, X_i, x_3, X_i, x_2\}.$$

This, however, reduces to a four-cycle $\{X_i, x_3, X_i, x_2\}$. To guarantee that the result of a concatenation is irreducible requires the original orbits to be primary. The following two results follow directly from definition 2.5.

Lemma 2.1. *The concatenation of two distinct primary hidden cycles is irreducible.*

Proof. If two hidden cycles can be concatenated then they must both contain an iterate on the same discontinuity X_i. So we may write two distinct primary cycles of some periods p and q as $O_x = \{X_i, x_2, x_3, \ldots, x_p\}$ and $O_y = \{X_i, y_2, y_3, \ldots, y_q\}$. Concatenating these as in definition 2.5 forms a distinct cycle $O_{xy} = \{X_i, \ldots, x_p, X_i, \ldots, y_q\}$ of period $p+q$. Because O_x and O_y are primary the term X_i appears precisely twice in sequence O_{xy}. Assume O_{xy} is reducible, then it must contain a repeating subsequence, which we can write as some $O_z = \{X_i, \ldots\}$, then since X_i appears twice this subsequence must be $O_z = O_x = O_y$, but O_x and O_y are distinct so this is false, hence O_{xy} is irreducible. □

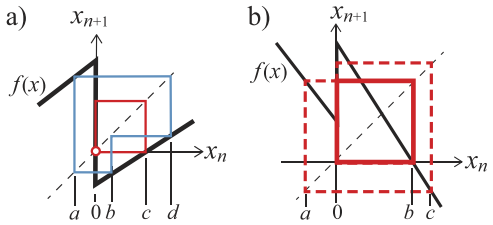

Figure 2. Illustrations of theorem 2.1: (a) a map with a three-cycle, hidden fixed point and hidden two-cycle, and hence hidden k-cycles for every integer k; (b) a map with a hidden two-cycle and hidden four-cycle, and hence k-cycles for even integer k. For example take: (a) $f(x) = \frac{1}{2} - \frac{7}{10}\Theta(x) + \frac{4}{5}x$, where $a = -\frac{5}{61}$, $b = \frac{9}{61}$, $c = \frac{1}{4}$, $d = \frac{53}{122}$; (b) $f(x) = -\frac{3}{2}x + \frac{1}{2}(1 + \Theta(x))$, where $a = -\frac{1}{9}$, $b = \frac{2}{3}$, $c = \frac{20}{27}$.

Theorem 2.1. *If the connected map f has primary hidden cycles of periods p and q, both with one iterate at a point X_i where f has a vertical branch, then there exist countably many irreducible cycles of periods $ap + bq$ for all $a, b \in \mathbb{N}$, and uncountably many aperiodic hidden orbits.*

Proof. Take two symbols O_x and O_y. For any positive integers $a, b \in \mathbb{N}$, we can construct a string consisting of a symbols O_x and b symbols O_y that cannot be written as a repetition of any single subsequence of the string. Now let O_x and O_y be the two distinct hidden cycles $O_x = \{X_i, x_2, x_3, \ldots, x_p\}$ and $O_y = \{X_i, y_2, y_3, \ldots, y_q\}$ from lemma 2.1, then this string corresponds to an irreducible hidden cycle with a copies of the sequence $\{X_i, x_2, x_3, \ldots, x_p\}$ and b copies of the sequence $\{X_i, y_2, y_3, \ldots, y_q\}$, hence with period $ap + bq$. Moreover, there are uncountably many ways to arrange the symbols O_x and O_y in an infinite aperiodic binary sequence, constituting uncountably many aperiodic hidden orbits. □

Note in this proof that, for any $a, b \in \mathbb{N}$, we can of course form sequences containing a copies of the symbol O_x and b copies of the symbols O_y that *are* reducible, but the result relies only on there existing at least one non-periodic sequence that gives an irreducible cycle. It is obvious that such a sequence always exists (and moreover the number of such sequences is known, and grows to infinity with the length, $n = a + b$, of the sequence, see e.g. [1, 28]).

Below we will derive two important corollaries of this result, but first let us illustrate it with two examples. Take the map in figure 2(a), with a regular three-cycle $\{a, d, b\}$. Were this a continuous map, Sharkovskii's theorem would imply the existence of k-cycles for all $k \in \mathbb{N}$, but this map has no other regular cycles. Instead it has a hidden fixed point $\{0\}$ and hidden two-cycle $\{0, c\}$. By theorem 2.1 with $p = 1$ and $q = 2$, concatenations of these generate irreducible cycles of every period $k = a + 2b$ for all $a, b \in \mathbb{N}$, i.e. k-cycles for every $k \in \mathbb{N}$. The most obvious are $\{0\}$, $\{0, c\}$, $\{0, 0, c\}$, $\{0, 0, 0, c\}$, etc.

The map in figure 2(b), on the other hand, has no odd period hidden cycles, but it has a hidden two-cycle $\{0, b\}$ and four-cycle $\{0, c, a, b\}$. By theorem 2.1, concatenations of these generate irreducible k-cycles where $k = 2a + 4b$ for all $a, b \in \mathbb{N}$, i.e. for every even $k \in \mathbb{N}$. The most obvious are $\{0, b\}$, $\{0, c, a, b\}$, $\{0, b, 0, c, a, b\}$, $\{0, b, 0, b, 0, c, a, b\}$, etc.

Directly from theorem 2.1 we have the following.

Corollary 2.1. *The existence of primary hidden cycles of two different periods, through the same discontinuity, implies chaos.*

By 'chaos' here we mean in the usual sense for one-dimensional maps as in [21]. As an extreme example, if $X_i \in F_i$ then there is a hidden fixed point at $x = X_i$, so any periodic sequence $\{X_i, x_2, x_3, \ldots, x_n\}$, with $n \geqslant 2$, can be concatenated with the period 1 sequence $\{X_i\}$ repeatedly to create hidden cycles of any period $p > n$. Immediately this implies the following.

Corollary 2.2. *If there exists a hidden fixed point $\{X_i\}$ and a hidden two-cycle $\{X_i, x_2\}$ with $x_2 \neq X_i$, then there exist irreducible cycles of every period.*

Proof. Concatenate the fixed point $\{X_i\}$ with itself, repeated any number of times, say $p-2$ for some $p > 2$. Then concatenate this with the two-cycle $\{X_i, x_2\}$ where $x_2 \neq X_i$. This creates an infinite set of hidden cycles each with the form $\{X_i, \ldots, X_i, x_2\}$, where the first $p-1$ iterates $x_1 = x_2 = \ldots = x_{p-1} = X_i$ can be repeated any number of times $p - 1 \in \mathbb{N}$. Moreover the fact that the last iterate is unique means each of these is irreducible. □

Hence the existence of a hidden two-cycle and a hidden fixed point at the same discontinuity implies chaos.

The proof is sufficient to show existence of irreducible cycles of every period, but clearly there also exist countably many other cycles with other forms, namely consisting of concatenations of sequences $\{X_i, \ldots, X_i, x_2\}$ of different lengths. Note how the notion of an irreducible cycle remains important, so for example $\{X_i\}$ is an irreducible cycle, but any repetition of it, $\{X_i, \ldots, X_i\}$, is not irreducible, while the sequence $\{X_i, \ldots, X_i, x_n\}$ is irreducible for any $n \in \mathbb{N}$ provided $x_n \neq X_i$.

The result in theorem 2.1 and its corollaries may seem trivial since they rely on concatenations of the different orbits that all pass through a point of discontinuity X_i, especially in corollary 2.2 where a cycle $\{X_i, x_2\}$ is concatenated any number of times with the point $\{X_i\}$ to obtain all periods. We shall see why the result is not trivial in the next section, where we consider how the concatenations relate to cycles in the limits of continuous maps.

We remark that the results here do not actually require F_i to be a connected set, relying solely on the existence of hidden cycles of a given period or periods, but in the following sections we will assume F_i is connected.

3. Perturbation to continuous maps

To help make sense of the result in theorem 2.1 let us focus on the implication that 'periods $1 + 2$ imply chaos' in corollary 2.2. Specifically, let us ask how it can be consistent with the contrary 'period 3 implies chaos' of continuous maps. This also serves to illustrate how hidden dynamics can be used to approximate the dynamics of maps with steep segments.

Consider the connected map $x_{n+1} = f(x_n)$, from (2), to be the limit of a continuous map $x_{n+1} = g(x_n, \omega)$ as some ω tends to infinity. A general method to define such 'regularisations' of connected maps was given in [17]. Essentially it replaces a vertical jump in (2) by a steep segment with approximate slope $\pm\omega$, and we will define such a function below.

We will show in theorem 3.1 that the existence of a hidden fixed point and hidden two-cycle in f implies the existence of a three-cycle, and hence all periods in g, for large enough ω. Conversely, we show that if a three-cycle of g exists, and has two iterates in a region where the gradient of g has order ω, then as $\omega \to \infty$ there exist a hidden fixed point and hidden two-cycle of f.

For completeness we will also show in theorem 3.2 that a hidden three-cycle persists under perturbation from $\omega \to \infty$. That is, a hidden three-cycle in f, implies the existence of a three-cycle (and hence all periods) in g, for large enough ω, and conversely, if a three-cycle of g exists, and has one iterate on a branch of g where its gradient has order ω, then as $\omega \to \infty$ the three-cycle tends towards a hidden three-cycle of f.

To formulate these results precisely we will consider a continuous piecewise-monotonic map that can be expressed, on some interval $U \subset \mathbb{R}$, in terms of three monotonic branches, f_R, f_ω, f_L, such that

$$x_{n+1} = g(x_n, \omega) = \begin{cases} f_R(x_n) & \text{if } x_n > \omega^{-1}, \\ f_\omega(x_n) & \text{if } 0 \leqslant x_n \leqslant \omega^{-1}, \\ f_L(x_n) & \text{if } x_n < 0, \end{cases} \tag{3}$$

where $f_L(0) = f_\omega(0)$ and $f_R(\omega^{-1}) = f_\omega(\omega^{-1})$. The map is therefore continuous, but not necessarily differentiable, at $x = 0$ and $x = \omega^{-1}$. (The functions f_R, f_L, f_ω, are differentiable on $\mathbb{R}$, or at least on sets enclosing their respective domains in (3).)

Taking $\omega \to \infty$ causes the middle branch f_ω to become steeper and ultimately vertical, such that (3) tends to the map

$$x_{n+1} = f(x_n) = \begin{cases} f_R(x_n) & \text{for } x_n > 0, \\ f_\infty(x_n) & \text{for } x_n = 0, \\ f_L(x_n) & \text{for } x_n < 0, \end{cases} \tag{4a}$$

where we define the limiting vertical branch at $x = 0$ as a set $\hat{F}$, writing

$$f_\infty(0) \in \hat{F} = [f_L(0), f_R(0)], \tag{4b}$$

and we will make use of the set F of which $\hat{F}$ is the closure, that is,

$$F = (f_L(0), f_R(0)). \tag{5}$$

We refer to (3) as the *continuous map*, and to (4) as the *connected map*. If we exclude f_∞ at $x = 0$ from the definition or define it as a single point (e.g. $f_\infty(0) = f_R(0)$), then we refer to (4a) alone as the *discontinuous map*. Only the connected map exhibits hidden dynamics.

3.1. Perturbation of a hidden two-cycle: periods 1 + 2 imply chaos

Assume (4) has a hidden fixed point and a hidden two-cycle. Without loss of generality, let this two-cycle be $\{0, {f_R}^{-1}(0)\}$. The alternative case $\{0, {f_L}^{-1}(0)\}$ is obtained by symmetry, and in fact in the following we will not need to consider the branch f_L, other than its boundary point $f_L(0) = f_\omega(0)$, and we may concern ourselves solely with f_R and f_ω.

Take the open set F defined in (5), constituting the vertical branch of the connected map, along with its successive pre-images G and H, according to

$$F = (f_L(0), f_R(0)), \qquad G = {f_\infty}^{-1}(F) = 0, \qquad H = {f_R}^{-1}(G), \tag{6}$$

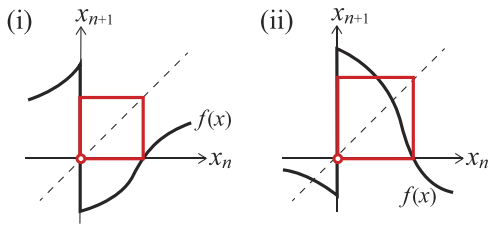

Figure 3. The two classes of connected map (4) that give the cycles with existence conditions (8) and (9), namely a hidden two-cycle (red square) and a hidden fixed point (red circle).

such that $H \to G \to F$ under (4). The existence conditions for a hidden fixed point and hidden two-cycle are then

$$\text{fixed point} \quad \Leftrightarrow \quad G \subset F, \tag{7a}$$

$$\text{2-cycle} \quad \Leftrightarrow \quad H \subset F. \tag{7b}$$

These can be translated into inequalities for the values of $f_L(0)$ and $f_R(0)$, and these fall into two classes depending on the sign of the slope of f_ω, or equivalently the sign of $f_R(0) - f_L(0)$:

- Class (i) illustrated in figure 3(i):

$$\text{fixed point} \quad \Leftrightarrow \quad f_R(0) < 0 < f_L(0), \tag{8a}$$

$$\text{2-cycle} \quad \Leftrightarrow \quad f_R(0) < {f_R}^{-1}(0) < f_L(0). \tag{8b}$$

- Class (ii) illustrated in figure 3(ii):

$$\text{fixed point} \quad \Leftrightarrow \quad f_L(0) < 0 < f_R(0), \tag{9a}$$

$$\text{2-cycle} \quad \Leftrightarrow \quad f_L(0) < {f_R}^{-1}(0) < f_R(0). \tag{9b}$$

By construction, in both classes the fixed point lies at $x = 0$, and the two-cycle has iterates $\{0, {f_R}^{-1}(0)\}$.

In theorem 3.1 we shall show that the hidden fixed point and two-cycle illustrated in figure 3, perturb to create the three-cycle illustrated in figure 4. Moreover we prove the converse, that the three-cycles in figure 4 collapse onto the hidden two-cycles in figure 3 as $\omega \to \infty$.

Theorem 3.1. *The existence of a hidden fixed point and hidden two-cycle in the connected map* (4)*, implies the existence of a three-cycle in the continuous map* (3) *for large enough* ω*. Conversely, the existence of a three-cycle with two iterates on the steep middle branch in the continuous map* (3)*, implies the existence of a hidden fixed point and hidden two-cycle in the connected map* (4)*, in the limit* $\omega \to \infty$*.*

Proof. Take the sets $G, H \subset F$ defined in (6), where $G = {f_\infty}^{-1}(F) = 0$ and $H = {f_R}^{-1}(G)$, and assume the conditions (7). Since the pre-image of F is a single point, ${f_\infty}^{-1}(F) = 0$, the same is true for the subset $G \subset F$, so let us also define $I = {f_\infty}^{-1}(H) = 0$. This implies $I = G$ and therefore $I \subset F$ (though this seems trivial we will use it in the next step). Now introduce a small perturbation of F given by the continuous set

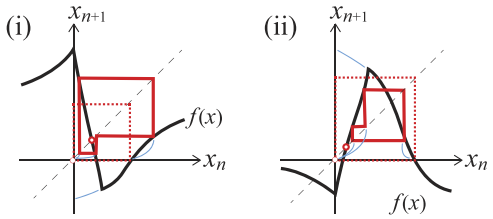

Figure 4. The two classes of continuous map (3) that tend to those in figure 3 as $\omega \to \infty$. A described in theorem 3.1, this shows a three-cycle (red orbit) and fixed point (red circle), tending to the hidden two-cycle (dotted red) and hidden fixed point (red circle) from figure 3.

$$F_\omega = \left(f_L(0), f_R(\omega^{-1})\right), \tag{10}$$

such that $F_\omega \to F$ as $\omega \to \infty$. Define perturbations of G, H, I, as $G_\omega = {f_\omega}^{-1}(F_\omega)$, $H_\omega = {f_R}^{-1}(G_\omega)$, and $I_\omega = {f_\omega}^{-1}(H_\omega)$. These sets are illustrated in figure 5 for the two cases where: (i) $f_L(0) > f_R(\omega^{-1})$, and (ii) $f_L(0) < f_R(\omega^{-1})$.

The size of the intervals G_ω and I_ω is of order ω^{-1}, so $G, H, I \subset F$ implies $G_\omega, H_\omega, I_\omega \subset F_\omega$ for large enough ω. Thus $I_\omega \subset F_\omega$ implies the map $f_\omega \circ f_R \circ f_\omega : I_\omega \to F_\omega$ has a fixed point, corresponding to a three-cycle of the map (3), which proves the first part of the theorem.

As a side remark, in addition to the three-cycle, $G_\omega \subset F_\omega$ implies the map $f_\omega : G_\omega \to F_\omega$ has a fixed point, giving a fixed point of the map (3), and $H_\omega \subset F_\omega$ implies the map $f_R \circ f_\omega : I_\omega \to F_\omega$ has a fixed point, corresponding to a two-cycle of the map (3). Clearly by similar construction one may obtain cycles of all periods.

Now, turning to the second part of the theorem, define the set F_ω by (10), and assume we can define pre-images $G_\omega, H_\omega, I_\omega$, such that

$$F_\omega \xrightarrow{{f_\omega}^{-1}} G_\omega \xrightarrow{{f_R}^{-1}} H_\omega \xrightarrow{{f_\omega}^{-1}} I_\omega. \tag{11}$$

Note in particular that

$$G_\omega = {f_\omega}^{-1}(F_\omega) = \left(0, \omega^{-1}\right) \tag{12}$$

is the domain of the function f_ω. Since we can also apply f_ω to I_ω, this must also lie in the domain of f_ω, so

$$I_\omega \subseteq G_\omega. \tag{13}$$

We will now argue that each of $G_\omega, H_\omega, I_\omega$, is a non-empty subset of F_ω for large ω. First, we assume for the theorem that there exists a three-cycle of (3) corresponding to a fixed point of the map $f_\omega \circ f_R \circ f_\omega : I_\omega \to F_\omega$, therefore the sets $F_\omega, G_\omega, H_\omega, I_\omega$, as they obey (11), are non-empty. Applying f_ω to (13) implies $H_\omega \subseteq F_\omega$, and since ${f_\omega}^{-1}$ is contracting with order ω^{-1}, for large enough ω this becomes $H_\omega \subset F_\omega$. The fact that the map $f_\omega \circ f_R \circ f_\omega : I_\omega \to F_\omega$ has a fixed point implies that the intersection $F_\omega \cap I_\omega$ is non-empty, and since $I_\omega \subseteq G_\omega$ by (13), this implies the intersection $F_\omega \cap G_\omega$ is non-empty. The size of the interval G_ω is of order ω^{-1}, so for large enough ω this implies $G_\omega \subset F_\omega$. Hence moreover $I_\omega \subseteq G_\omega \subset F_\omega$.

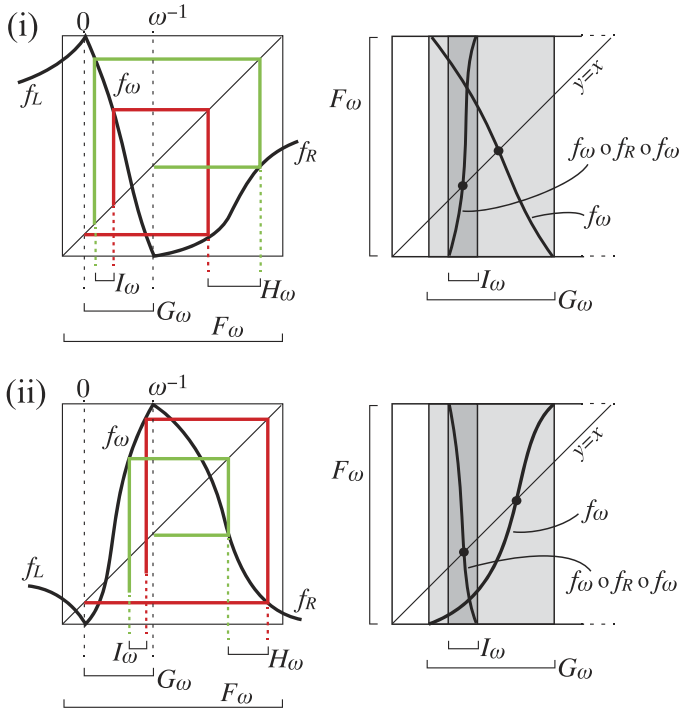

Figure 5. The two classes of the map (3) showing the intervals $F_\omega, G_\omega, I_\omega$, and an illustration of the intermediate value theorem applied to the maps on $G_\omega \to F_\omega$ and $I_\omega \to F_\omega$, implying the existence of a fixed point and three-cycle. In the limit $\omega \to \infty$ the classes (i)–(ii) correspond to the maps in figure 3.

Thus for large enough ω we have $G_\omega, H_\omega, I_\omega \subset F_\omega$. As we then take the limit $\omega \to \infty$, we have directly that $F_\infty = F$ with $G_\infty = I_\infty = G$ and $H_\infty = H$, therefore $G, H, I \subset F$, giving us the existence conditions (7) for the existence of a hidden fixed point and hidden two-cycle in the connected map (4). □

Note from this proof that since the size of the interval G_ω shrinks as ω^{-1}, the hidden fixed point and two-cycle lie ω^{-1} close to the three-cycle of the continuous map for large ω.

We can illustrate the proof more explicitly by taking the two cases $f_L(0) > f_R(\omega^{-1})$ and $f_R(\omega^{-1}) > f_L(0)$ separately, as in figure 4. This shows the fixed point and three-cycle tending towards the hidden fixed point and two-cycle as $\omega \to \infty$, as described in the first half of the proof of theorem 3.1. To illustrate the proof more explicitly, first take the case $f_L(0) > f_R(\omega^{-1})$, then $G_\omega \subset F_\omega$ implies $f_R(\omega^{-1}) < 0 < \omega^{-1} < f_L(0)$, while $I_\omega \subset F_\omega$ implies $f_R(\omega^{-1}) < f_R{}^{-1}(0) < f_R{}^{-1}(\omega^{-1}) < f_L(0)$. As $\omega \to \infty$ these become $f_R(0) < 0 < f_L(0)$ and $f_R(0) < f_R{}^{-1}(0) < f_L(0)$, i.e. the conditions (8). In the other case, when $f_R(\omega^{-1}) > f_L(0)$, then $G_\omega \subset F_\omega$ implies $f_L(0) < 0 < \omega^{-1} < f_R(\omega^{-1})$, while $I_\omega \subset F_\omega$ implies $f_L(0) < f_R{}^{-1}(\omega^{-1}) < f_R{}^{-1}(0) < f_R(\omega^{-1})$. As $\omega \to \infty$ these become $f_L(0) < 0 < f_R(0)$ and $f_L(0) < f_R{}^{-1}(0) < f_R(0)$, i.e. the conditions (9).

We give some further geometric insight into how successively higher period cycles are formed in the continuous map as ω is perturbed away from ∞ in appendix A.2.

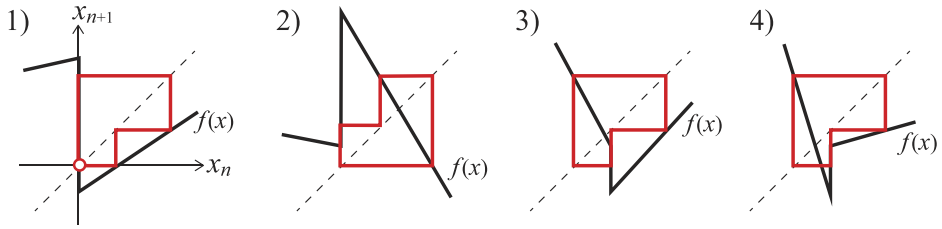

Figure 6. The four classes of hidden three-cycle in theorem 3.2. In class (1) there is also a hidden fixed point and two-cycle, in classes (2–4) there are no other cycles in the maps depicted, but by varying the left branch in 2–3 and the right branch in 4 a hidden fixed point and two-cycle can be introduced.

3.2. Persistence of a primary three-cycle

In the maps of theorem 3.1, a hidden fixed point and hidden two-cycle concatenate to form a non-primary hidden-3-cycle, which perturbs for finite ω into a regular three-cycle. For completeness, let us also give the corresponding result for a *primary* hidden three-cycle, which we show persists under perturbation to finite ω into a regular three-cycle, in which case of course we have the familiar 'period 3 implies chaos'.

There are four distinct topologies of the map (4) in which a primary hidden three-cycle appears, shown in figure 6, and defined by:

(a) $f_R(0) < f_L(0)$ and $f_R(0) < {f_R}^{-2}(0) < f_L(0)$,
(b) $f_R(0) > f_L(0)$ and $f_L(0) < {f_R}^{-2}(0) < f_R(0)$,
(c) $f_R(0) < f_L(0)$ and $f_R(0) < {f_L}^{-1} \circ {f_R}^{-1}(0) < f_L(0)$,
(d) $f_R(0) > f_L(0)$ and $f_L(0) < {f_L}^{-1} \circ {f_R}^{-1}(0) < f_R(0)$.

These are essentially delineated by the sign of $f_R(0) - f_L(0)$ (in classes 1 and 3 this sign is negative, in classes 2 and 4 this sign is positive), and which point of the cycle lies on the discontinuity point $x = 0$ (in classes 1–2 this is one of the outer iterates, in classes 3–4 this is the middle iterate). If an outer iterate of the cycle lies on $x = 0$, we can without loss of generality assume it is the leftmost iterate.

For these we have a similar result to that for a hidden two-cycle.

Theorem 3.2. *The existence of a primary hidden three-cycle in the connected map* (4)*, implies the existence of a three-cycle in the continuous map* (3) *for large enough* ω*, and vice versa. Conversely, the existence of a three-cycle with one iterate on the steep middle branch in the continuous map* (3) *as* $\omega \to \infty$*, implies the existence of a primary hidden three-cycle in the connected map* (4)*.*

The proof is similar to that of theorem 3.1, so we shall omit the details here, particularly since the result is unsurprising, merely showing that if a three-cycle is primary (has only one iterate on the discontinuity), then it persists in the large ω limit (whereas the three-cycle in theorem 3.1 had two iterates on the discontinuity). For the connected map we define the set $F = (f_L(0), f_R(0))$ and its pre-images G, H, I. For the continuous map we define the set $F_\omega = \left(f_L(0), f_R(\omega^{-1})\right)$ and its pre-images G_ω, H_ω, I_ω. Then $G = 0$ and $G_\omega = \left(0, \omega^{-1}\right)$ as before. There are two scenarios to consider. For the classes 1–2 defined above, we define H_ω and I_ω such that

$$F_\omega \xrightarrow{{f_\omega}^{-1}} G_\omega \xrightarrow{{f_R}^{-1}} H_\omega \xrightarrow{{f_R}^{-1}} I_\omega, \tag{14}$$

and for classes 3–4 we define H_ω and I_ω such that

$$F_\omega \xrightarrow{f_\omega{}^{-1}} G_\omega \xrightarrow{f_R{}^{-1}} H_\omega \xrightarrow{f_L{}^{-1}} I_\omega. \tag{15}$$

Using these, the proof of theorem 3.2 follows by steps very similar to those in theorem 3.1.

The results of this section can be relaxed to permit non-monotonic branches, provided we demand monotonicity in an ω^{-1}-neighbourhood of the iterates of the 2 and three-cycles, but the more limited result for piecewise-monotonic maps is sufficient for our interest here.

4. Applications to oscillatory systems

We used continuous maps in section 3 merely to help interpret the result that 'periods $1+2$ imply chaos', by relating hidden orbits to the limit of unstable orbits on a steep segment. Perhaps a more direct way to illustrate hidden orbits is by locating them in applications. Here we consider three examples, and for easy comparison we choose parameter values that give a similar map in each case, so each has a stable three-cycle, a hidden two-cycle, and a hidden fixed point. Later in section 5 we make some more general remarks on the interpretation of the hidden dynamics in these models and regularisations of them.

4.1. A toy hybrid oscillator

The following one degree of freedom oscillator forms a toy model for the two real applications that follow, and suggests how widely these phenomena may occur in general. Consider the hybrid oscillator

$$\dot{u}_1 = u_2, \qquad \dot{u}_2 = \alpha u_2 - u_1, \tag{16a}$$

$$u_2 \mapsto -\sqrt{-u_2} \quad \text{if } u_1 = 0, \quad u_2 < -2, \tag{16b}$$

and we shall take $\alpha = 0.09$. This represents a simple oscillator with a spring forcing and a negative damping, and a dissipative impact that occurs at a position $u_1 = 0$ if the velocity is below $u_2 = -2$, resulting in a drop in the speed u_2.

The oscillator is shown in phase space in figure 7. It is clear that orbits which hit the half-line $\{u_1 = 0, u_2 > -2\}$ evolve smoothly through it, while orbits that hit the half-line $\{u_1 = 0, u_2 < -2\}$ suffer an impact before continuing to evolve smoothly. However, orbits which hit $u_1 = 0$ precisely at $x_2 = -2$, which we say *graze* the threshold $u_2 = -2$, may either continue evolving according to (16a), or map according to (16b) before continuing to follow (16a).

Hidden dynamics describes what happens in the continuum between these two extremes at the discontinuity, by letting the grazing orbit evolve onwards from all states in the set $\left\{u_2 \in [-\sqrt{2}, -2], u_1 = 0\right\}$, forming the red region in figure 7 (left). These states are typically neglected, as they are not accessed by forward evolution of the model from states arbitrarily close to (but not on) the discontinuity.

A stable three-cycle of the oscillator is also shown in figure 7 (right).

We can define a return map $u_{2,n} \mapsto u_{2,n+1}$ on the half-line

$$\left\{(u_1, u_2) \in \mathbb{R}^2 : u_1 = 0 < u_2\right\}.$$

This is calculated numerically and shown in figure 8, and has a stable period 3 cycle, but no other regular cycles. The points c_0 and $c_\pm$ correspond to those in figure 7.

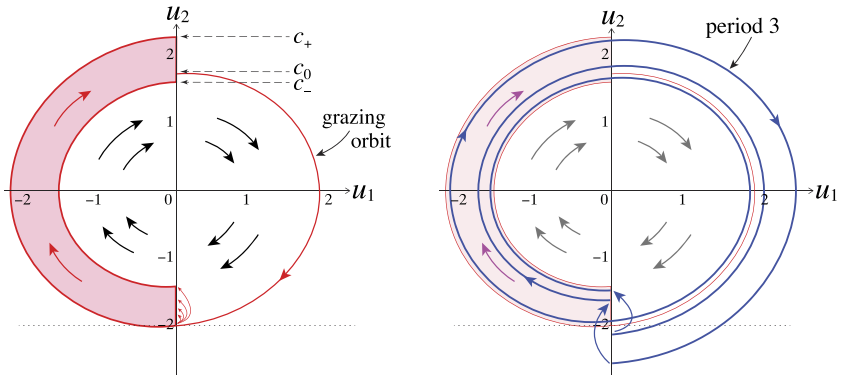

Figure 7. The oscillator in phase space. The left picture shows the grazing orbit, which passes through a point c_0 on the half-line $\{u_2 > 0, u_1 = 0\}$. From the point $(u_1, x_2) = (0, -2)$ this can follow one of two trajectories to return to $\{u_2 > 0, u_1 = 0\}$ at c_- (if (16b) is applied) or c_+ (otherwise)), and the red shaded region indicates the continuum of non-physical 'hidden' trajectories between these. The right picture shows a stable period 3 orbit that undergoes two impacts.

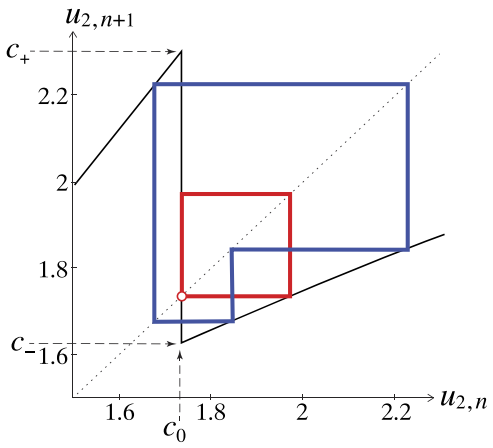

Figure 8. The Poincaré return map on $\{u_2 > 0, u_1 = 0\}$, showing a stable three-cycle with a hidden two-cycle and hidden fixed point. (The map is found by numerical simulation.)

Were this a continuous map, the existence of a three-cycle would imply the existence of cycles of all periods by Sharkovski's theorem. By theorem 2.1 we know these can be provided by hidden orbits. Indeed, it is easy to see that this map has a hidden fixed point and hidden two-cycle, as shown in figure 8.

In figure 9 we illustrate the hidden period 1 cycle corresponding to the fixed point of the map, and the hidden two-cycle, in a figure corresponding to figure 7. Both can be found by following the grazing orbit back from the discontinuity threshold until it returns to the red 'hidden' zone. Note that the period 1 orbit is a subset of the period 2. (Note also the fixed point, two-cycle, and three-cycle, co-exist, we plot them on separate figures only for clear visibility.)

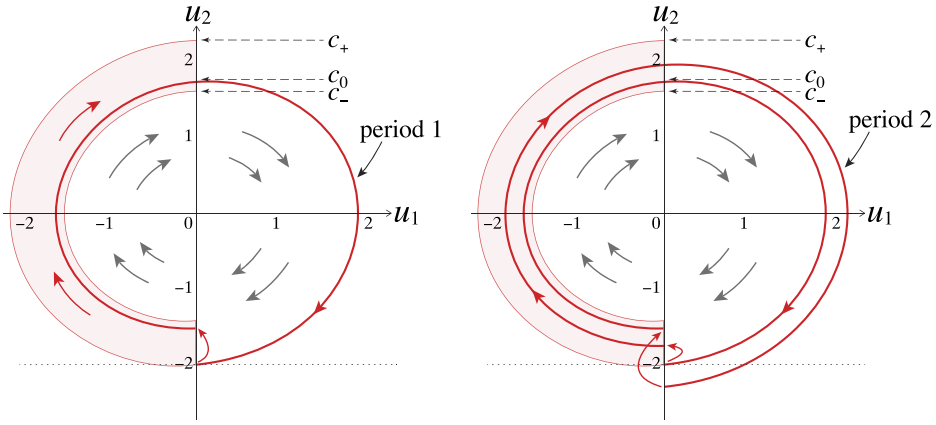

Figure 9. The hidden fixed point (left) and hidden two-cycle (right) in the oscillator, in the same space as figure 7.

In figure 10 we plot these cycles against time. The displacement $u_1(t)$ and speed $u_2(t)$ are shown for the three-cycle (showing one complete cycle), and for the hidden two-cycle over the same duration, showing one and a half complete cycles. At $t \approx 12.5$ the u_2 coordinate is seen grazing the threshold $u_2 = -2$, at which it can turn around and continue as a smooth curve, or can impact according to (16b). The short dotted vertical line indicates the range of theoretical values lying between these two extremes, corresponding to the vertical branch in the map in figure 8, which the physical system cannot access. From one of these values, a trajectory can continue on and evolve through one further oscillation in which an impact occurs, and then the orbit returns to the grazing trajectory, forming the period 2 oscillation.

4.2. Application to yeast growth

The growth and mitosis of a yeast cell is modelled in [9] by an oscillatory reaction of three chemical concentrations (u_1, u_2, u_3), along with the cell mass m, as

$$\begin{aligned}
\dot{u}_1 &= k_1 - k_2' u_1 - k_2'' u_1 u_2,\\
\dot{u}_2 &= \frac{(k_3' + k_3'' u_3)(1-u_2)}{J_3 + 1 - u_2} - \frac{k_4 m u_1 u_2}{J_4 + u_2},\\
\dot{u}_3 &= k_5' + k_5'' \frac{(mu_1)^n}{J_5^n + (mu_1)^n} - k_6 u_3,\\
\dot{m} &= rm\Big(1 - \frac{m}{M}\Big).
\end{aligned} \tag{17a}$$

The mass undergoes a division event representing mitosis as u_1 drops below a threshold value, given by

$$m \mapsto m/2 \quad \text{if } u_1 = 1/10, \quad \dot{u}_1 < 0. \tag{17b}$$

Here we take the various parameters as $k_1 = 0.04$, $k_2' = 0.152$, $k_2'' = 1$, $k_3' = 1$, $k_3'' = 10$, $k_4 = 35$, $k_5' = 0.005$, $k_5'' = 0.2$, $k_6 = 0.1$, $J_3 = 0.04$, $J_4 = 0.04$, $J_5 = 0.3$, $n = 4$, $r = 0.01$, $M = 10$, based on values of Michaelis–Menten reaction coefficients in [9].

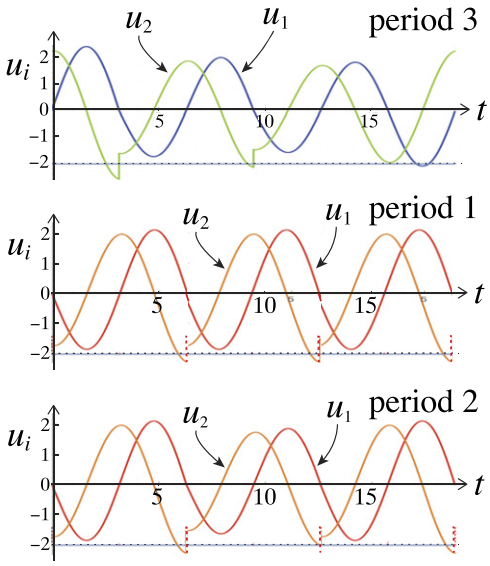

Figure 10. Graphs of the stable three-cycle (showing one complete cycle), hidden period 1 cycle (showing three complete periods), and hidden two-cycle (showing one and a half complete periods). The dashed red line shows the set $u_2 \in [-2, -\sqrt{2}]$ which generates the vertical branch at the discontinuity.

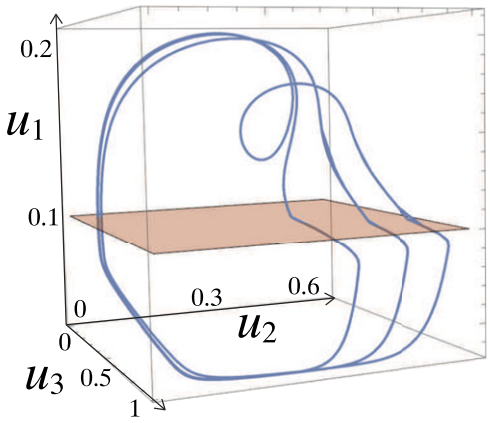

Figure 11. A stable three-cycle of the yeast cell cycle.

A typical cycle in (u_1, u_2, u_3) space is shown in figure 11, depicting a stable three-cycle found for these parameter values.

It was observed in [16] that near the threshold $u_1 = \frac{1}{10}$ on the region where $\dot{u}_1 > 0$, trajectories appear to crowd up, such that near the attractor (in this case near the three-cycle in figure 11) they can be approximated by a one-dimensional return map in the mass

$$m_{n+1} = f(m_n) \quad \text{on} \left\{ (m, u_1, u_2, u_3) \in \mathbb{R}^4,\ u_1 = \frac{1}{10},\ \dot{u}_1 > 0 \right\}. \tag{18}$$

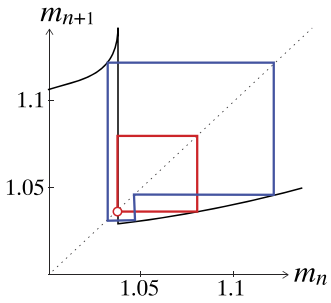

Figure 12. The dynamics approximately reduces to a one-dimensional map in the mass m. For the parameters given above we see a three-cycle, plus a hidden two-cycle and hidden fixed point. (The map is found by numerical simulation.)

This map is shown in figure 12, and was obtained by simulation, taking an initial point $(u_1, u_2, u_3) = (0.1, 0.2635, 0.3371)$ near the attractor, and then varying initial points m_n, to calculate the return point m_{n+1}. We note that this is only an approximation of the higher dimensional dynamics, but it was shown in [16] to be sufficient to understand the qualitative periodic behaviour of the four-dimensional model (17).

The discontinuity in this map is due to the two qualitatively different return paths observable in figure 11: the left branch of the map describes orbits that make a loop above $u_1 = \frac{1}{10}$ and thereby allow longer for m to grow between divisions, the right branch describes orbits with no loop, and the discontinuity occurs where an orbit forms a loop that grazes the threshold $u_1 = \frac{1}{10}$.

First observe that this map has a stable three-cycle, and no other regular cycles at these parameter values. Similarly to the toy model in section 4.1, as a connected map on the interval, we may therefore conjecture that it has hidden cycles of period 1 and 2. It is easily seen from the map in figure 12 that a hidden two-cycle exists, along with a hidden fixed point, whose concatenations create hidden cycles of all periods.

Although the one-dimensional map here is only an approximation for the four-dimensional system, we do indeed find this hidden cycle in the full model. In figure 13 we plot the oscillation of u_1, and the growth-and-division of the mass m, for these two cycles. The upper picture shows two complete cycles of the three-cycle. The lower two picture show the hidden period 1 and two cycles over the same time interval, executing a little more than six and three complete cycles, respectively.

As in the toy oscillator the hidden cycles are, by definition, not normally considered to be accessible trajectories of the physical system from any typical initial condition, but they pass through the continuum of states across its discontinuity. Just after $t \approx 0$ we see m increasing and u_1 decreasing. At $t \approx 8.5$ the orbit arrives at the discontinuity, where we see that u_1 lies tangent to the threshold $u_1 = \frac{1}{10}$. At this point the cycle can either continue growing us u_1 turns around and begins increasing again (the trajectory marked $\circ 1$ in figure 13), or the cell can divide according to (18) (the trajectory marked $\circ 2$ in figure 13). Between $\circ 1$ and $\circ 2$ there exist a continuum of hidden orbits—trajectories that the physical system is usually assumed not to evolve through from a typical initial condition—corresponding to points on the vertical branch of the map in figure 12, and one of these (marked $\circ 3$ in figure 13) evolves to connect back up to the grazing trajectory, and form the cycle.

The system in section 4.1 was conceived as a simplification of this model, with the same essential features of oscillations stabilised by a discontinuous loss in one variable: speed in

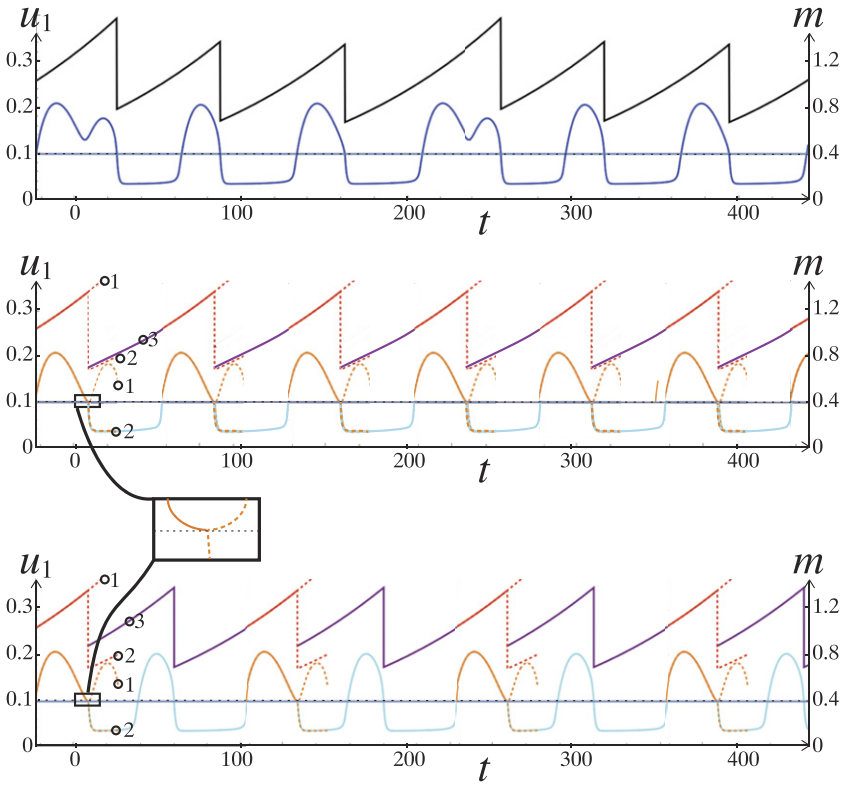

Figure 13. The three-cycle (upper figure, showing two complete periods), the hidden period 1 cycle (middle graph, showing just over six complete cycles), and the hidden two-cycle (lower figure, showing just over three complete cycles). '○1' and '○2' label trajectories corresponding to the extremes of the vertical branch of the map, '○3' labels the trajectory between these that forms the hidden cycle.

the toy model (16a) and mass in the yeast model. The system (17a) is itself a simplification of a nine dimensional model which shows similar dynamics, but the simpler model here is sufficient for illustration.

4.3. Application to human sleep-wake cycles

A recent application shown to exhibit rich dynamics associated with circle maps with discontinuities arises from studies into the regulation of sleep-wake homeostasis [5]. We shall show that this system also has hidden cycles. In addition, this application illustrates a non-trivial choice of how the vertical branch must be chosen at the discontinuity.

The model consists of two processes controlling homeostatic sleep pressure. The pressure decreases during sleep as a function $H_{\text{sleep}}(t)$, and increases while awake as a function $H_{\text{wake}}(t)$, according to

$$\begin{aligned} H_{\text{sleep}}(t,t_0) &= H^+(t)\mathrm{e}^{(t_0-t)/k_{\text{s}}},\\ H_{\text{wake}}(t,t_0) &= 1-\big(1-H^-(t)\big)\mathrm{e}^{(t_0-t)/k_{\text{w}}}. \end{aligned} \tag{19}$$

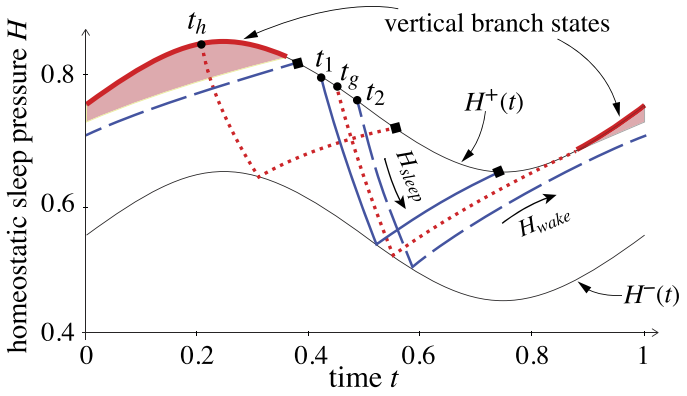

Figure 14. Homeostatic pressure cycling between sleep and wake, switching at the circadian thresholds (black sinusoidal curves). A hidden orbit is shown starting from $t = t_g$, grazing the threshold (dotted red curve), creating a region of inaccessible states (red shaded area), and departing from some point $t = t_h$ inside the inaccessible region. Two regular orbits are shown slightly either side of the grazing orbit, from initial conditions $t = t_1$ (full blue curve) and $t = t_2$ (dashed blue curve), showing the discontinuity between their end points. The start and end points of each trajectory are shown by black dots and squares, respectively.

The change in homeostatic pressure switches between these at two oscillating circadian thresholds, with falling asleep occurring when H_{wake} reaches a threshold H^+, and waking occurring when H_{sleep} reaches a threshold H_-, where

$$H^{\pm}(t) = H_0^{\pm} + a\,\sin(2\pi t). \tag{20}$$

These sinusoidal thresholds and resulting homeostatic trajectories are illustrated in figure 14. For this illustration we take parameter values $a = 0.1$, $H_0^+ = 0.75$, $H_0^- = 0.55$, $k_{\text{s}} = 0.25$, $k_{\text{w}} = 0.8$, similar to those in [5]. Three examples of orbits that begin on the sleep threshold $H^+(t)$ are shown. Two regular orbits are shown starting at some $t = t_1$ (full blue curve) and $t = t_2$ (dashed blue curve), passing through one sleep and one wake interval each. The duration of these orbits differs markedly because they lie just either side of $t = t_g \approx 0.445$, from which the orbit (red dashed) grazes the sleep threshold at around $t \approx 0.87$. The 'end point' of the orbit starting from t_g could be considered to be either of the two points at the extremes of the red 'inaccessible' region, but we will also permit it to lie on the continuum of states between these (indicated by thick red curve segment on the $H^+(t)$ threshold). We also illustrate an orbit starting from a point t_h inside this inaccessible region (dotted red curve).

The observation from [5] is that the return map to the sleep threshold $H^+(t)$, let us call it $T(t)$, is a circle map that can contain discontinuities due to the presence of grazing. This map takes some t_n to $t_{n+1} = T(t_n)$, by going from the sleep threshold at time t_n, to the wake threshold at time t_-, and then back to sleep threshold at time $T(t_n)$. Thus $T(t_n)$ obtained by solving the two equations $H_{\text{wake}}(T, t_-) = H^+(T)$ and $H_{\text{sleep}}(t_-, t_n) = H^-(t_-)$ for the functions $T : [0, 1) \to [0, 1)$ and $t_- : [0, 1) \to [0, 1)$.

The map is shown in figure 15, and was found by numerical calculation. Orbits corresponding to those in figure 14 are shown. The map has a discontinuity where the sleep-wake cycles grazes the sleep threshold, again illustrated by the orbit starting from $t = t_g \approx 0.445$ (dotted red line from t_g), and mapping to a vertical branch that corresponds to the inaccessible region

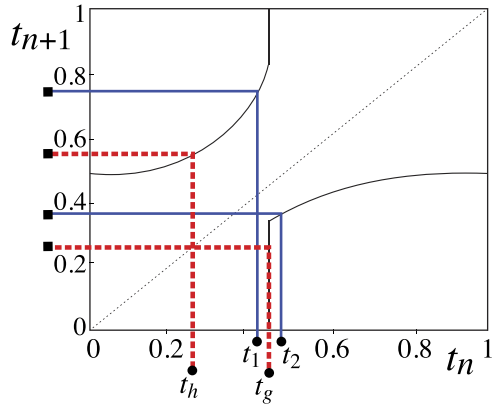

Figure 15. The return map to the surface $H = H^+(t)$, showing orbits corresponding to those in figure 14. The vertical branch has been drawn through the cyclic boundary $t = 0$–1, through the states that are inaccessible due to the discontinuity in the red region of figure 14. The map is found by numerical calculation.

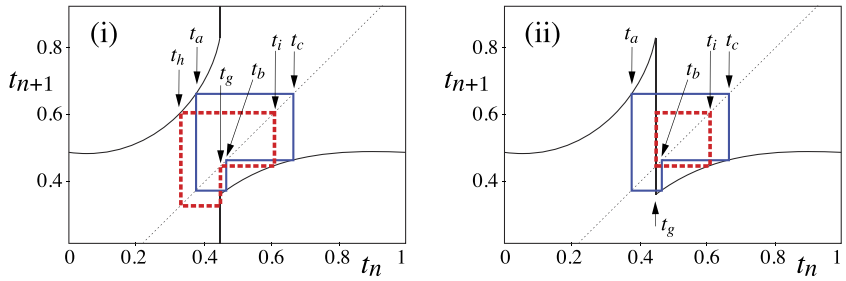

Figure 16. Hidden cycles of a discontinuous map obtained from a model of sleep-wake regulation. The vertical branch is either drawn: (i) upward from the left branch, giving a hidden three-cycle, or (ii) downward from the left branch, giving a hidden two-cycle and fixed point.

in figure 14. We will return to how this vertical branch is drawn in the next paragraph. Hidden orbits are those that have iterates on the vertical branch, among the inaccessible states in figure 14. One such orbit is shown mapping from $t = t_g$, through one iteration to $t = t_g$, and through one more iteration to around $t \approx 0.55$ (red dashed lines).

Now note that, as T is a circle map, there are two possible ways to connect its branches across the discontinuity. As shown in figure 15, we can either: (i) draw the vertical branch upward from the left branch so it passes through the boundary at $t = 0$–1, or perhaps more obviously, (ii) draw the vertical branch downward from the left branch. Only one of these is appropriate to the sleep-wake model, and to determine which, one has to consider the continuous time system figure 14 the map was derived from, to find which choice of vertical branch describes states that are passed through on the homeostatic thresholds at the discontinuity. These states, the red region in figure 14, consists of the states $t \in (0.85, 1) \cup (0, 0.36)$ (or more simply $t \in (0.85, 1.36)$ as this is a circle map). Comparing to figure 16 we see that the appropriate map is figure 16(i), and hence the vertical branch as drawn in figure 14, in which the discontinuity point $t_g \approx 0.445$ maps to the vertical branch $t \in (0.85, 1) \cup (0, 0.36)$.

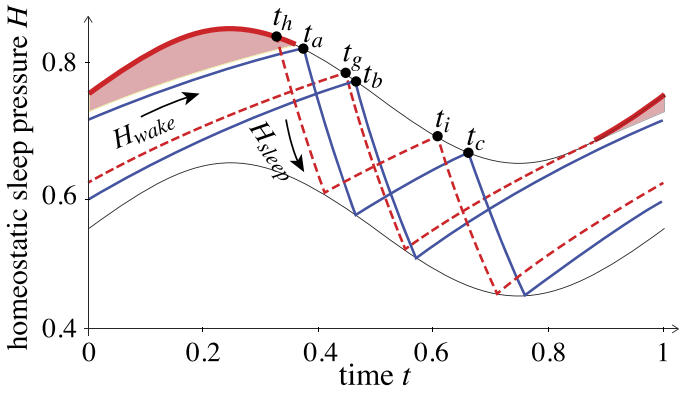

Figure 17. The three-cycle and hidden three-cycle from figure 16(i), correspond to stable and unstable sleep-wake cycles in the model of homeostatic regulation from [5]. The times indicated on the sleep threshold correspond to those in figure 16.

As shown in figure 16, the map has a regular three-cycle $\{t_a, t_b, t_c\}$ (existing independent of the vertical branch). If we form the vertical branch as in (i) it also has a hidden three-cycle $\{t_g, t_h, t_i\}$. By contrast, the incorrect formulation in (ii) has a hidden fixed point $\{t_g\}$ and hidden two-cycle $\{t_g, t_i\}$. As a result, the map in (ii) has hidden cycles of all periods by corollary 2.2. The map in (ii), however, has only these two three-cycles, and is a counterexample to Sharkovski's theorem for circle maps.

In figure 17 we show the sleep-wake cycles corresponding to the map cycles from figure 16(i), namely the three-cycle (full blue saw-tooth curve), and the hidden three-cycle (dashed red saw-tooth curve). One may easily observe that the hidden cycle from figure 16(ii) has no corresponding cycle in the continuous time sleep-wake dynamics, thus the manner in which the vertical branch is taken, and the existence of hidden orbits in the map, is not arbitrary.

So we see here that when a discontinuity occurs in a map defined on the circle, there are two ways to connect it, and which of those is appropriate is determined by the application. We will make more general remarks about how such connections can be formed in appendix A.1. Note in figure 16 that the two types of connected map are closely related, because the pre-images of the discontinuity that define hidden orbits are the same, up to points where those pre-images re-intersect the vertical branch. For example, the hidden three-cycle in figure 16(i) has iterates at $t = t_g \approx 0.445$, $t \approx 0.61$, and $t \approx 0.33$, while the iterates of the hidden two-cycle in figure 16(ii) also lie at $t = t_g \approx 0.445$ and $t \approx 0.61$; which of these forms a valid orbit is determined by the definition of the vertical branch.

5. Hidden cycles: interpretation and applications

In section 4 we saw examples of hidden orbits within physical applications. The hidden orbits form a continuous family of trajectories connecting orbits either side of a discontinuity. They can be followed in backward time in the system from the discontinuity, and thereby form closed cycles through the discontinuity. They have learnt the term 'hidden' as they are not normally considered to be accessible in the forward time evolution from a given initial condition.

We have concentrated on low period cycles for the purposes of illustration. As we change parameters in any of the maps and models in this paper, these cycles can undergo bifurcation that produce cascades of cycles of higher periods. The papers [15, 18] took a first look at the role that hidden orbits play in 'filling the gaps' in different kinds of bifurcation diagrams, connecting to stable branches much as standard unstable cycles would. For instance in [15] it is shown that border collision bifurcations can be interpreted as flip and fold border collision bifurcations involving hidden orbits.

The study of the role of hidden cycles in the bifurcations of applications like those in section 4 remains to be done. In [16] the cell cycle—in both its 4 and 9 dimensional models—was shown to exhibit a period incrementing cascade as the parameter k_2' varies. One should be able to obtain the hidden cycles that fill the gaps in those bifurcation diagrams, something we leave for future interest.

Systems like those in section 4, where a 'hard' impact is modelled as a discontinuity, can be thought of as setting a boundary problem, before and after impact, for a more complete model that would describe the temporal and spatial variations of the oscillator *through* the moment of impact. Such a *regularisation* could take many forms (see e.g. chapter 12 of [14]). The simplest kind of regularisation is a smoothing of the model's equations, as we considered in section 3, where we saw how hidden orbits and their concatenations correspond to regular unstable orbits of a continuous map in some limit. More generally, regularisations may involve a variety of physical complexities that are approximated by the discontinuity, such as delays, hysteresis, or stochasticity in where and when the discontinuity occurs, or with change occurring on fast timescales or small spatial scales rather than actually being discontinuous.

We can expect that in any regularisation there exists some unstable object that is approximated by the hidden dynamics, but importantly, hidden orbits exist independent of such regularisations, permitting the study of unstable cycles that approximate the dynamics of those more complex systems, within the idealisation of the discontinuous model.

A more interesting consequence of these results is that we can use theorem 2.1 to infer the existence of regular cycles in a smooth map with a steep segment.

For an example take the map depicted in figure 18, and consider this to approximate a map with a steep segment in the region $|x| < \omega$ for some large ω. Now assume we know this map has a hidden three-cycle $\{a, e, c\}$, as shown. Applying Sharkovskii's theorem to the continuous map would imply there must exist cycles of all periods, but it is easy to see that these cannot all be hidden, in particular there is no hidden fixed point or hidden two-cycle. Therefore there must exist a regular fixed point $\{b\}$ and two-cycle $\{a, d\}$, for some $a, b, d \neq 0$. Indeed we find this to be the case (of course for this simple example they are very easy to see by inspection), i.e. the presence of the hidden three-cycle correctly predicts the existence of a regular fixed point and two-cycle, as shown in figure 18.

More generally, consider a discontinuous map, or a continuous map well approximated by it, in which the only regular cycle has period p. The implication of theorem 2.1 is then that every period $k \prec p$ must exist as a hidden cycle. Conversely, if the only hidden cycle in a discontinuous map (or continuous map approximated by it) has period p, and the periods $k \prec p$ do not exist as hidden cycles, then they must exist as regular cycles.

So hidden orbits permit us to approximate steep segments with discontinuities, and importantly to do so without any loss of solutions in the singular limit where the map's slope becomes infinite. In that limit, orbits overlap, but remain well-defined through hidden orbits and their concatenations. The advantage is that, in many situations, it may be analytically or numerically more tractable to solve a map with a vertical branch than a map with a steep nonlinearity.

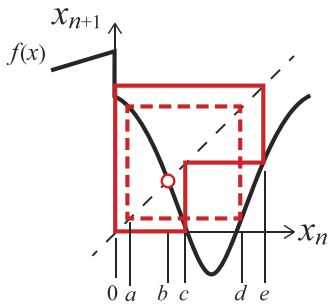

Figure 18. Existence of a hidden three-cycle implies existence of a regular fixed point and two-cycle. For example let $f(x) = 2 + x - \left(\frac{2}{5} + x + 2\,\mathrm{sech}\,3(x-1)\right)\Theta(x)$, then $a = 0.156$, $b = 0.572$, $c = 0.769$, $d = 1.284$, $e = 1.508$. This map approximates, for example, $g(x,\omega) = \frac{9}{5} + \frac{x}{2} - (\frac{1}{5} + \frac{x}{2})\tanh(\omega x) - (1 + \tanh(\omega x))\mathrm{sech}(3(x-1))$ for large ω.

6. Closing remarks

Until recently the behaviours of continuous and discontinuous maps have seemed far removed, the latter able to exhibit bifurcations and periodicities not limited by the laws constraining continuous maps, and as such a whole new field of dynamical theory has sprung up to organise the zoology of *discontinuity-induced bifurcations* for maps (see e.g. [4, 7, 22, 27], in parallel to similar theory for flows [7, 10, 11, 14]). We see here that connected maps provide a kind of unification between discontinuous and continuous maps. The introduction of hidden orbits changes none of the results derived previously, but in providing an underpinning framework of unstable orbits, it does restore some of the intuitive geometry and even some of the most profound theorems familiar from continuous maps.

Other works have attempted to extend Sharkovkii's theorem to maps with discontinuities in other ways. Recently in [17] it was shown that a discontinuous map can be blown-up into a continuous one, in a manner that preserves kneading invariants and hence periodicities, implying that the discontinuous map must also contain the cycles guaranteed by the Sharkovskii ordering.

It was shown in [15], for example, that by introducing hidden orbits, the bifurcations of discontinuous maps become qualitatively similar to those of continuous maps. In [17] it was shown in general how one can regularise a discontinuous map, by first connecting it with a vertical branch, and then blowing-up the pre-images of the discontinuity in a manner that preserves kneading invariants and hence periodicities. This implies that the discontinuous map must also contain the cycles guaranteed by the Sharkovskii ordering, and that 'period three implies chaos' should apply to discontinuous maps. The corollaries 2.1 and 2.2 suggest more peculiar results associated with a vertical branch, captured in the notion that 'periods $1 + 2$ imply chaos'.

A study for multi-valued maps in [2, 3], motivated by 'applications to differential equations without uniqueness conditions', showed that Sharkovkii's theorem holds only in a restricted form if applied to *primary* orbits, which are allowed to visit a set-valued point only once, in contrast to corollary 2.2 if we include all hidden orbits and their concatenations.

In section 5 we saw moreover an example of how, using the results of sections 2 and 3, hidden orbits can be used to infer the existence of regular orbits, and even to infer the existence of orbits of continuous maps with steep segments.

Therefore, though hidden orbits are inherently unstable, and might not be readily observable, as with other unstable orbits this does not preclude their usefulness, whether seeking to understand the periodicities of a map as in this paper, to understand the unstable objects propping up their otherwise 'gappy' bifurcation diagrams as in [15, 18], or to understand their relation to continuous maps as in [17]. It is not so much the hidden cycles themselves that have significance as physical trajectories, but rather the points outside the discontinuity that they connect into a *hidden* periodic structure, strung out through pre-images of the point of discontinuity, that plays a crucial role in organising the map's dynamics, both hidden and regular.

Appendix A.

A.1. A note on types of connected map

In the example of the sleep-wake model in section 4.3, due to the periodicity of the circadian cycle, the map was defined on a circle. This made it possible for a vertical branch to connect the map at the discontinuity in two different ways.

In general, given any map with a discontinuity at some X_i, there are infinitely many different ways to connect its branches to form a connected map, through different choices of the set F_i in (2b). Any hidden cycles are a property of the particular connected map for a given choice of F_i.

Nevertheless, for a given discontinuous map, it is easy to see that the connected map associated with it will fall into certain qualitative types. For one discontinuous map, figure 19 shows three possible ways to connect it, labelled as 'simple', 'cyclic', or 'spiky'. In any of these cases hidden orbits exist through the vertical branches. The first is the simple connection formed by the vertical branch across its discontinuity, $F_i = \left[f_+(X_i), f_-(X_i)\right]$. Alternatively, if the map is cyclic on a finite or infinite domain which maps to the circle, then the connection can be made by passing through those cyclic boundaries. Lastly, the connection does not have to be contained between the branches and instead can be 'spiky'.

The sleep-wake model in section 4.3 provided an example of a 'cyclic' connection across a discontinuity, where we saw how the appropriate connection was determined by the application.

The 'spiky' type of connection is, it turns out, unavoidable. Some applications permit set-valued spikes even in continuous maps that are set-valued at certain points, for example as in the last image in figure 19.

Given any discontinuity, the 'spiky' map turns out to be inevitable when studying higher iterates. Figure 20 shows a map $x_{n+1} = f(x_n)$ (left graph) with a simple connecting branch, along with its second iterate $x_{n+2} = f^2(x_n)$ (right graph) which exhibits a spike. As an example take the connected map

$$x_{n+1} = \begin{cases} f_R(x_n) = -1 + x_n & \text{if } x_n > 0, \\ f_\infty(x_n) \in [-1, +1] & \text{if } x_n = 0, \\ f_L(x_n) = 1 - x_n & \text{if } x_n < 0, \end{cases} \tag{21}$$

illustrated in figure 20. For this we have $f(0) \in f_\infty(0) = [-1, +1]$. The second iterate at $x_n = 0$ is then

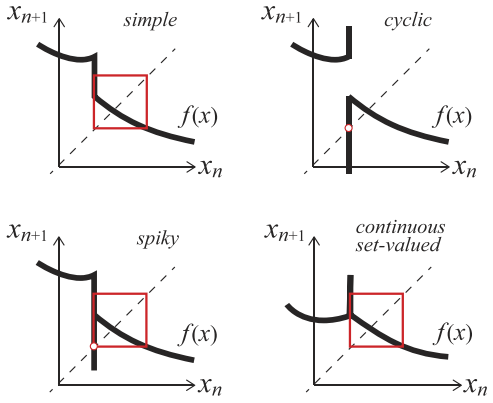

Figure 19. Different kinds of vertical branches creating hidden cycles: a 'simple' connection in a map with a gap, or the same map connected across a 'cyclic' domain, or with a 'spiky' connection. Lastly, maps can be set-valued even without jumps in value (see e.g. the 'M-maps' as considered in [2, 3]. The maps have hidden two-cycles and/or fixed points as shown.

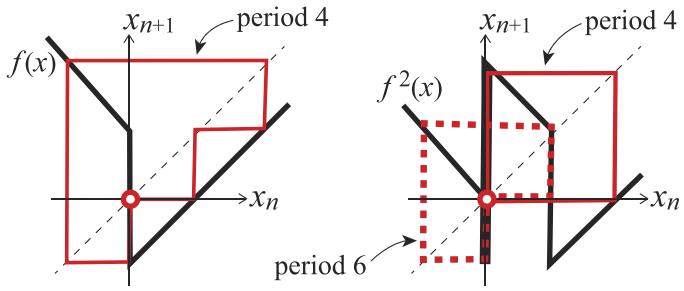

Figure 20. A piecewise-continuous map f (left) and its second derivative f^2 (right), showing that if $x_{n+1} = f(0) \in [-1,+1] = [f(0+), f(0-)]$ then $x_{n+2} = f^2(0) \in [-1,2]$, which is larger than $\left[f^2(0-), f^2(0+)\right] = [0,2]$. Left: the map f showing the hidden fixed point C and hidden four-cycle. Right: the map f^2, showing hidden a four-cycle and hidden six-cycle of f.

$$f^2(0) \in f(f_\infty(0)) = f_L([-1,0]) \cap f_\infty(0) \cap f_R([0,+1])$$
$$= [1,2] \cap [-1,+1] \cap [-1,0] = [-1,2]$$

which, as shown one the right of figure 20, produces a spike at $x_n = 0$. Note that no such spike occurs at the other discontinuity of the map f^2 at $x_n = 1$.

This further illustrates that the values a map takes at a discontinuity are not arbitrary. In this case the range of values of higher derivatives of a map is larger than the obvious vertical branch $\left[f^2(0-), f^2(0+)\right]$ interpolated across the discontinuity, but is nevertheless well-defined by the range of the original map f.

Figure 20 also illustrates how concatenations of hidden cycles are observed in maps and their higher iterates. In the left of figure 20 we illustrate a hidden fixed point and hidden four-cycle of f. Through concatenations, there should therefore exist cycles of every higher period. In the map f^2 on the right of figure 20, of course, we can only observe cycles of even period.

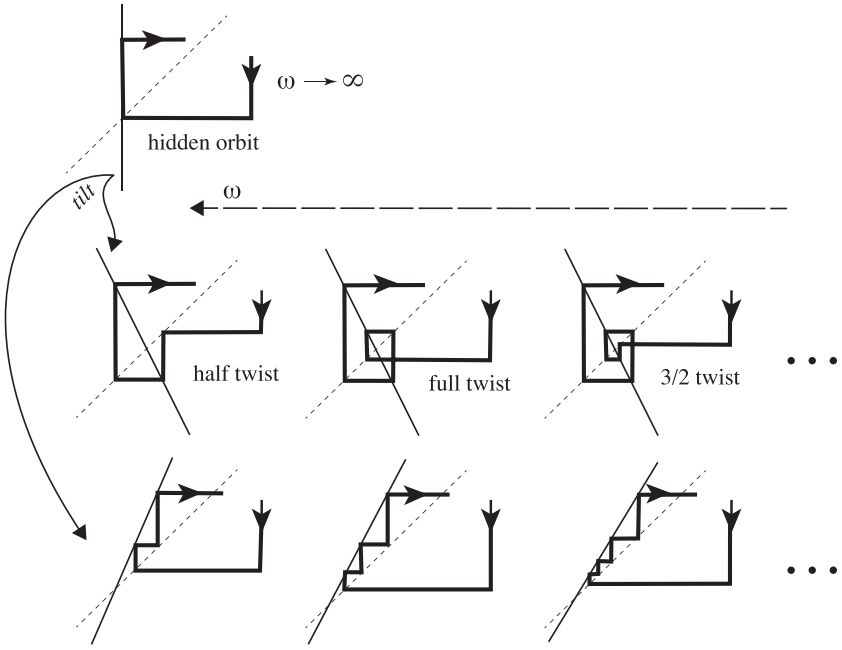

Figure 21. 'Regularisations' of a hidden cycle near the fixed point. The concatenations of the fixed point $\{0\}$ become regular cycles twisting around or stepping away from a fixed point, depending on the slope of the steep segment, $k = \text{sign}(f_\omega)$. In the limit $\omega \to \infty$ these crowed up in an ω^{-1} neighbourhood of the hidden fixed point.

Here we illustrate both the four-cycle (a two-cycle of f^2), and a six-cycle (dashed, a three-cycle of f^2). Note the six-cycle includes a point outside $[0, 2]$ at $x = 0$, and moreover contains points on both discontinuities.

While it is necessary to draw attention to the different forms that a connected map may take, it is beyond our scope here to derive a complete classification of the topologies of connected maps, or a complete theory of hidden cycles in them. However, theorem 2.1 directly tells us that whatever the form of the connected map, if it possesses primary hidden cycles with period p and q, then it also possesses irreducible hidden cycles of all periods $ap + bq$ for any $a, b \in \mathbb{N}$.

A.2. Twisting to form infinite periods

Theorem 2.1 tells us that if a connected map has a hidden fixed point and two-cycle, then it has cycles of all periods by concatenation. This is consistent with applying Sharkovskii's theorem to the perturbed map (3), namely that there must then exist cycles of every period, and they lie, like the three-cycle found in theorem 3.1, near the hidden two-cycle that exists in the limit $\omega \to \infty$. Depending on the sign of the jump they make either integer or half integer rotations around the fixed point on the steep segment, adding an even or odd number of iterates within $\mathcal{O}(1/\omega)$ of the hidden fixed point, depending on the slope of f_ω, as illustrated in figure 21.

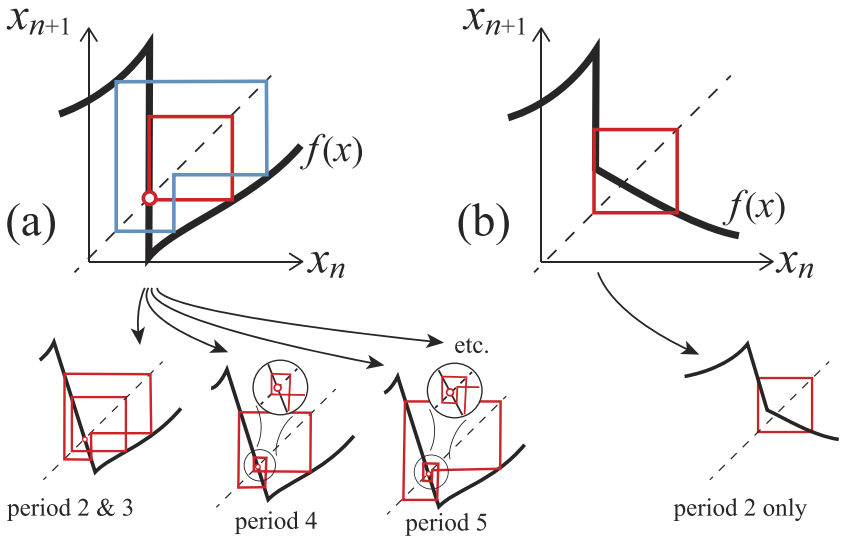

Figure 22. A connected map and its perturbation to a continuous map, showing: (a) map with a three-cycle (blue), and all other periods are provided by concatenations of a hidden two-cycle (red square) and a hidden fixed point (red circle); (b) map with a regular fixed point and a hidden two-cycle (red square), but no other odd periods. Below: in a continuous map the period 2 perturbs to all periods 2, 3, 4, 5, ... in (a), but to period 2 only in (b) due to the lack of the hidden fixed point.

In figure 22 we illustrate how this twisting generates cycles of successively higher periods in the continuous map, using the map from figure 3(i) in (a), and a similar map but without a fixed point in (b), defined on an interval. In (a) the hidden cycles generate all periods consistent with theorem 3.1. In (b) there is no hidden fixed point so theorem 3.1 does not apply.

ORCID iDs

Mike R Jeffrey https://orcid.org/0000-0002-3325-7211
Viktor Avrutin https://orcid.org/0000-0001-7931-8844

References

[1] Allouche J-P and Shallit J 2003 *Automatic Sequences* (Cambridge: Cambridge University Press)
[2] Andres J, Fiser J and Jüttner L 2002 On a multivalued version of the Sharkovskii theorem and its application to differential inclusions *Set-Valued Anal.* **10** 1–14
[3] Andres J, Jüttner L and Pastor K 2005 On a multivalued version of the Sharkovskii theorem and its application to differential inclusions: II *Set-Valued Anal.* **13** 47–68
[4] Avrutin V, Gardini L, Sushko I and Tramantona F 2019 *Continuous and Discontinuous Piecewise-Smooth One-Dimensional Maps* (*Nonlinear Science Series A* vol 95) (Singapore: World Scientific)
[5] Bailey M P, Derks G and Skeldon A C 2018 Circle maps with gaps: understanding the dynamics of the two-process model for sleep-wake regulation *Eur. J. Appl. Math.* **29** 845–68
[6] Chin W, Ott E, Nusse H E and Grebogi C 1994 Grazing bifurcations in impact oscillators *Phys. Rev.* E **50** 4427–44

[7] di Bernardo M, Budd C J, Champneys A R and Kowalczyk P 2008 *Piecewise-Smooth Dynamical Systems: Theory and Applications* (Berlin: Springer)
[8] di Bernardo M, Garefalo F, Glielmo L and Vasca F 1998 Switchings, bifurcations, and chaos in dc/dc converters *IEEE Trans. Circuits Syst.* I **45** 133–41
[9] Fall C P, Marland E S, Wagner J M and Tyson J J 2002 *Computational Cell Biology* (New York: Springer)
[10] Filippov A F 1988 *Differential Equations with Discontinuous Right-Hand Sides* (Dortrecht: Kluwer) (original in Russian 1985)
[11] Glendinning P 2016 Classification of boundary equilibrium bifurcations of planar Filippov systems *Chaos* **26** 013108
[12] Guckenheimer J and Williams R F 1979 Structural stability of Lorenz attractors *Publ. Math. IHÉS* **50** 59–72
[13] Hös C and Champneys A R 2012 Grazing bifurcations and chatter in a pressure relief valve model *Physica* D **241** 2068–76
[14] Jeffrey M R 2019 *Hidden Dynamics: The Mathematics of Switches, Decisions, & Other Discontinuous Behaviour* (Berlin: Springer)
[15] Jeffrey M R and Avrutin V 2021 Bifurcations of hidden orbits in discontinuous maps *Nonlinearity* **34** 6140–72
[16] Jeffrey M R and Dankowicz H 2014 Discontinuity-induced bifurcation cascades in flows and maps with application to models of the yeast cell cycle *Physica* D **271** 32–47
[17] Jeffrey M R and Glendinning P 2021 Hidden dynamics for piecewise smooth maps *Nonlinearity* **34** 3184–98
[18] Jeffrey M R and Webber S 2020 The hidden unstable orbits of maps with gaps *Proc. R. Soc.* A **476** 20190473
[19] Jiang H, Chong A S E, Ueda Y and Wiercigroch M 2017 Grazing-induced bifurcations in impact oscillators with elastic and rigid constraints *Int. J. Mech. Sci.* **127** 204–14
[20] Lee C M, Collins P J, Krauskopf B and Osinga H M 2008 Tangency bifurcations of global Poincaré maps *SIAM J. Appl. Dyn. Syst.* **7** 712–54
[21] Li T-Y and Yorke J A 1975 Period three implies chaos *Am. Math. Mon.* **82** 985–92
[22] Nordmark A B 1997 Universal limit mapping in grazing bifurcations *Phys. Rev.* E **55** 266–70
[23] Palis J and de Melo W 1982 *Geometric Theory of Dynamical Systems* (Berlin: Springer)
[24] Pring S R and Budd C J 2010 The dynamics of regularized discontinuous maps with applications to impacting systems *SIAM J. Appl. Dyn. Syst.* **9** 188–219
[25] Sharkovskii A N 1964 Co-existence of cycles of a continuous mapping of the line into itself *Ukrainian Math. J.* **16** 61–71
Sharkovskii A N 1995 Co-existence of cycles of a continuous mapping of the line into itself *Int. J. Bifurcation and Chaos* **5** 1263–73 (Engl. transl.)
[26] Shi J, Guldner J and Utkin V I 1999 *Sliding Mode Control in Electro-Mechanical Systems* (Boca Raton, FL: CRC Press)
[27] Simpson D J W 2016 Border-collision bifurcations in $\mathbb{R}^N$ *SIAM Rev.* **58** 177–226
[28] Sloane N J A The on-line encyclopedia of integer sequences oeis.org/A027375 last viewed 15 September 2021
[29] Tramantona F and Westerhoff F 2016 Piecewise-linear maps and their application to financial markets *Front. Appl. Math. Stat.* **2** 1–10
[30] Williams R F 1979 The structure of Lorenz attractors *Publ. Math. IHÉS* **50** 73–99
[31] Yang J Y 2017 Cherry flow: physical measures and perturbation theory *Ergod. Theory Dyn. Syst.* **37** 2671–88